ANALYSIS OF 3D AND 4D PROTON TREATMENT PLANNING FOR HEPATIC TUMORS
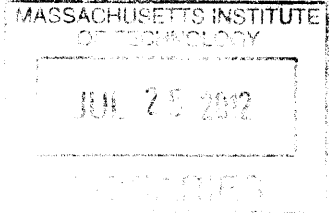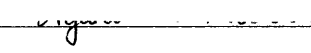
By

Agata Elżbieta Wiśniowska

SUBMITTED TO THE DEPARTMENT OF NUCLEAR SCIENCE
AND ENGINEERING
IN PARTIAL FULFILLMENT OF THE REQUIREMENTS FOR THE DEGREE OF

BACHELOR OF SCIENCE IN NUCLEAR SCIENCE AND ENGINEERING
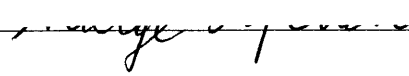AT THE
MASSACHUSETTS INSTITUTE OF TECHNOLOGY

JUNE 2011

Agata Wiśniowska. All Rights Reserved.

The author hereby grants to MIT permission to reproduce and to distribute publicly
Paper and electronic copies of this thesis document in whole or in part.

Signature of Author: _____

Agata Wiśniowska
Department of Nuclear Science and Engineering
May 19th, 2011

Certified by: _____

Richard Lanza
Senior Research Scientist, Department of Nuclear Science and Engineering
Thesis Supervisor

Certified by: _____

George T.Y. Chen
Professor of Radiation Oncology, Harvard Medical School
Thesis Reader

Accepted by: ____ _____

Dennis Whyte
Professor of Nuclear Science and Engineering
Chairman, NSE Committee for Undergraduate Students

ANALYSIS OF 3D AND 4D PROTON TREATMENT PLANNING FOR HEPATIC TUMORS

By

Agata Elżbieta Wiśniowska

Submitted to the Department of Nuclear Science and Engineering on May 19th, 2011
In partial Fulfillment of the Requirements for the Degree of
Bachelor of Science in Nuclear Science and Engineering

ABSTRACT

The purpose of this study is to assess the difference between 4D liver dose calculations versus standard 3D treatment planning and to investigate the dosimetric gain of gating on radiation dose to normal tissue. 4DCT scans are collected for 25 patients with hepatic tumors treated by proton radiotherapy. The 4D treatment planning process explicitly takes into account respiratory motion of abdominal organs. A 4DCT scan consists of 10 3D anatomical states, each at an instant of time in the respiratory cycle. 4D treatment planning includes 1) propagating the target contours, drawn by a physician on one phase, to all breathing phases using deformable registration, 2) calculating the compensating bolus for proton therapy, and then 3) calculating 4D dose distributions. Dose volume histograms are used to compute the effective uniform dose (EUD) delivered to normal liver.

We found that 4DCT planning always results in a larger EUD to normal liver when compared with dose from a 3DCT plan. The mean EUD difference between 4D and 3D planning is 3.8Gy (σ=1.9Gy, $p<0.0001$). Gated 4D treatment planning results in a lower EUD to normal liver compared to ungated planning, with a mean difference of 2.9 Gy (σ=1.9Gy, $p<0.0001$). The EUD difference is only weakly correlated with the magnitude of the superior-inferior (S-I) tumor motion (r=0.59 for 4D/3D, r=0.48 for ungated/gated). The ΔEUD correlation with clinical target volume (CTV) (as fraction of liver volume) is much weaker (r=0.31 for 4D/3D, r=0.26 for ungated/gated). There was no evidence that the tumor position within the liver influenced the ΔEUD. This study suggests that physicians should consider 4D treatment planning if the risk of normal tissue complications is high. Normal tissues may also be significantly spared by gated treatment as a motion management strategy.

Thesis Supervisor: Richard Lanza

Title: Senior Research Scientist

INTRODUCTION

Radiation treatment for malignancies has been used for over 100 years since the discovery of X-rays in 1895 by Wilhelm Roentgen. Radiation therapy refers to the medical use of ionizing radiation to treat malignant tumors in patients. As radiation transits tissue, it deposits energy in both normal and diseased tissues, resulting in biological effects. The desired effect is killing tumor cells; an undesired side-effect is damage to normal tissues.

Accurate calculation of the dose delivered to normal tissue is crucial for effective radiation therapy: underestimating normal tissue exposure can lead to treating patients with doses higher than is safe, which could lead to radiation-associated injury to the liver (13), while overestimating healthy tissue irradiation can overconstrain how much radiation can be delivered to the tumor and lower tumor control probability. Accuracy of dosimetry to normal tissue is especially important for dose escalation studies, which often prescribe doses near the maximum dose tolerated by normal tissue in such studies as (14).

In addition to random setup variations during fractionated treatment (15), respiratory motion poses a challenge for effective treatment. This problem can be addressed by organ motion reduction strategies. In principle, tumor irradiation could be delivered at breath-hold to minimize tumor movement (16): this method has been reported to be better than irradiation during free respiration (17). Breath hold during treatment, however, has its limitations because the breath hold reproducibility is an issue: it is difficult for the patients to consistently hold their breath for the duration of the treatment. Moreover, this varies from patient to patient, introducing a large uncertainty in tumor position for treatment planning.

3

While some groups argue that tumor motion has negligible effect on photon treatment planning (dose volume histograms (DVHs)) (e.g., 18), others consider liver motion an important issue and include it in their calculations (19). Conventional 3D treatment planning based on a single CT scan, does not explicitly consider tumor motion during treatment. Rosu *et al.* (20) modeled both geometric uncertainties in photon treatment and 1D (superior-inferior) tumor motion to account for breathing, and found that 3DCT-based treatment planning both underestimated and overestimated the dose to normal tissue as compared to their 4D planning model. Their model used mathematical convolution of a static dose distribution with a motion kernel as an approximation of 4D movement instead of the actual 4D calculation for each breathing phase. Additionally, Rosu's group assumed rigid structure contours instead of propagating the contours drawn for one breathing phase to all other phases using deformable registration.

In this study, we examine the question of how 4D treatment planning (TP) differs in estimating the dose to normal tissues from 3DTP. 4DCT scans are used in 4DTP to quantify tumor and normal tissue motion. Unlike Rosu, we are interested in calculating the impact of motion on proton beam radiotherapy. This study is clinically relevant because patients are being treated with protons at MGH. The advantage of proton therapy in treatment of hepatic tumors is that it has been reported to reduce the normal liver irradiated as compared to photons (21).

4DCT data comprise separate CT scans taken over the course of the breathing cycle (ten scans equally spaced in breathing cycle phases T00–T90), and allow accurate determination of the dose delivered to the tumor and surrounding tissue as the organ of interest moves with the patient's breathing. In contrast with the limited 1D movement considered in previous studies (20), we use the

4D treatment planning software Aqualyzer (22) to account for full three-dimensional effects of breathing (i.e., superior-inferior, anterior-posterior, and right-left organ movement), and use Plastimatch deformable registration (24) to propagate tumor contours from the phase in which they were drawn to all other breathing phases based on tissue density differences. While a similar tool exists (32) that takes 3D sets of data at different respiratory phases, propagates the contours, and performs the calculation on each data set, Aqualyzer had many additional features that facilitated data analysis, such as customized structures, movies of organ motion during breathing, and summary of structure motion.

BACKGROUND

The earliest treatments used photon beams to irradiate tumors. Photon energy deposition to tissue peaks close to the skin and then decays in an exponential manner (see Figure **1**). Thus skin and tissues close to the skin receive the highest dose even though most frequently the actual tumor lies much deeper in the body. Because of exponential attenuation, the beam continues irradiating tissues past the tumor.
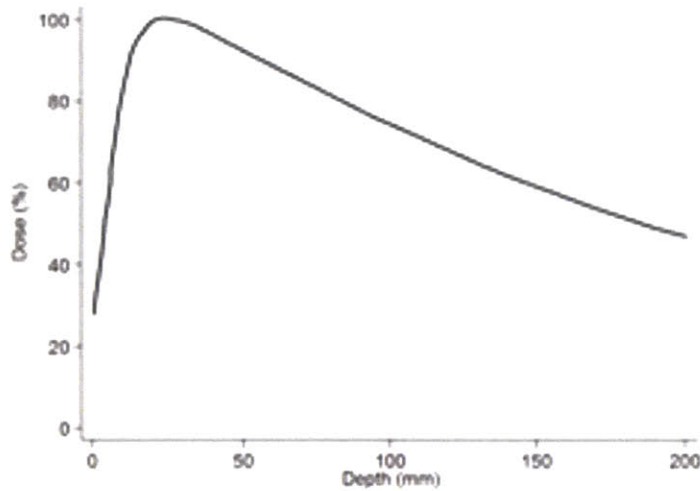
Figure 1. Photon dose deposition as a function of tissue depth in mm. The maximal dose is deposited close to the skin region; the dose exponentially decays in deeper tissues; figure adapted from (1)

Irradiating too much of normal tissue poses a risk. If excessive radiation is applied to normal tissues in addition to irradiating the tumor, radiation-induced injury may develop. Some organs are particularly radiation sensitive, e.g., the gastrointestinal tract (5), and the treatments are designed to avoid these sensitive regions.

While a single photon beam can deliver the prescribed dose, it will also significantly irradiate any tissue on the way, as shown in Figure **2**. To deliver a high dose to the tumor and to reduce dose to adjacent normal tissues, multiple beams are used. If we introduce a second beam (orthogonal to the first one, as shown in part B of Figure **2**), then the normal tissue receives only 50% of the total dose while the tumor still receives the prescribed dose. The tradeoff is that in this case, more normal tissue is irradiated (as shown in Figure **2**).
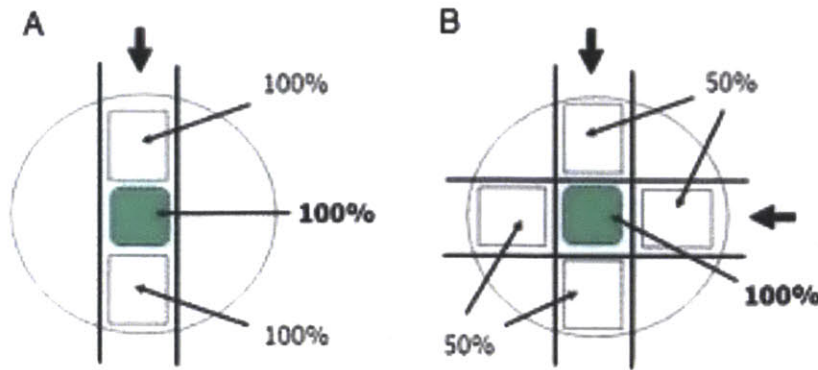
6

Figure 2. Photon dose deposition in the body. A: One beam delivers 100% of the dose to both the tumor (in green) and to normal tissue (white regions). B: Two orthogonal beams each carrying 50% of the dose: as a result the normal tissue receives 50% of the dose while the tumor still receives 100% of the dose; figure adapted from (6)

Conformal radiotherapy, with uniformly illuminated fields being convergent, generally only results in convex high dose regions (as in Figure 2). Uniform beams cannot be easily used to form concave dose distributions, where there is a cold region (e.g. spinal cord) within a U shaped target (e.g. tumor that is U shaped and has a critical dose limiting structure within the U). In the 1990's, a more advanced delivery method was developed to produce concave distributions, named intensity-modulated radiation therapy (IMRT), which typically uses 5-7 intensity modulated photon beams (2). Figure 3 shows the principle of IMRT. Here, there are 5 beams in the example, each entering from a different angle. Each beam covers the tumor width, but has a non-uniform (i.e., intensity modulated) beam profile. The cumulative dose from all five fields delivers the prescribed dose to the tumor, but also can spare a critical structure adjacent to the target (rectum in the example below).
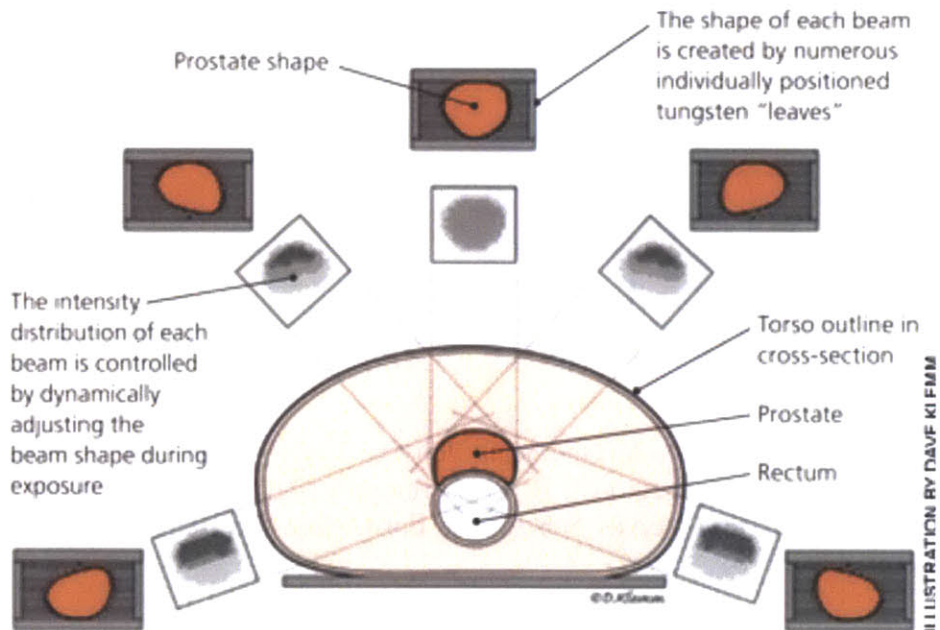
Figure 3. Sample IMRT beam setup. Five beams are shown pointed at centrally located tumor (prostate). The beams are dynamically adjusted to create a convex shape on the bottom of the tumor to save an important structure (rectum); adapted from (3)

The inherent disadvantage of photon radiation therapy is that photons deposit energy throughout their path in the body, damaging normal tissue in addition to tumor. One solution is to use a different type of ionizing radiation, specifically protons. Protons are charged and unlike photons have a rest mass. As a result they have much higher probability for interaction with matter. As a high energy proton enters the tissue, it deposits energy minimally, but as it slows down, its energy deposition as a function of depth (dE/dx) rapidly increases and then decreases before it comes to rest. Energy loss for charged particles is described by the Bethe-Bloch equation which shows a rapid increase in energy deposition with decreasing particle velocity, resulting in a characteristic rapid increase near the end of range, usually referred to as the Bragg peak (see Figure 4) (4).
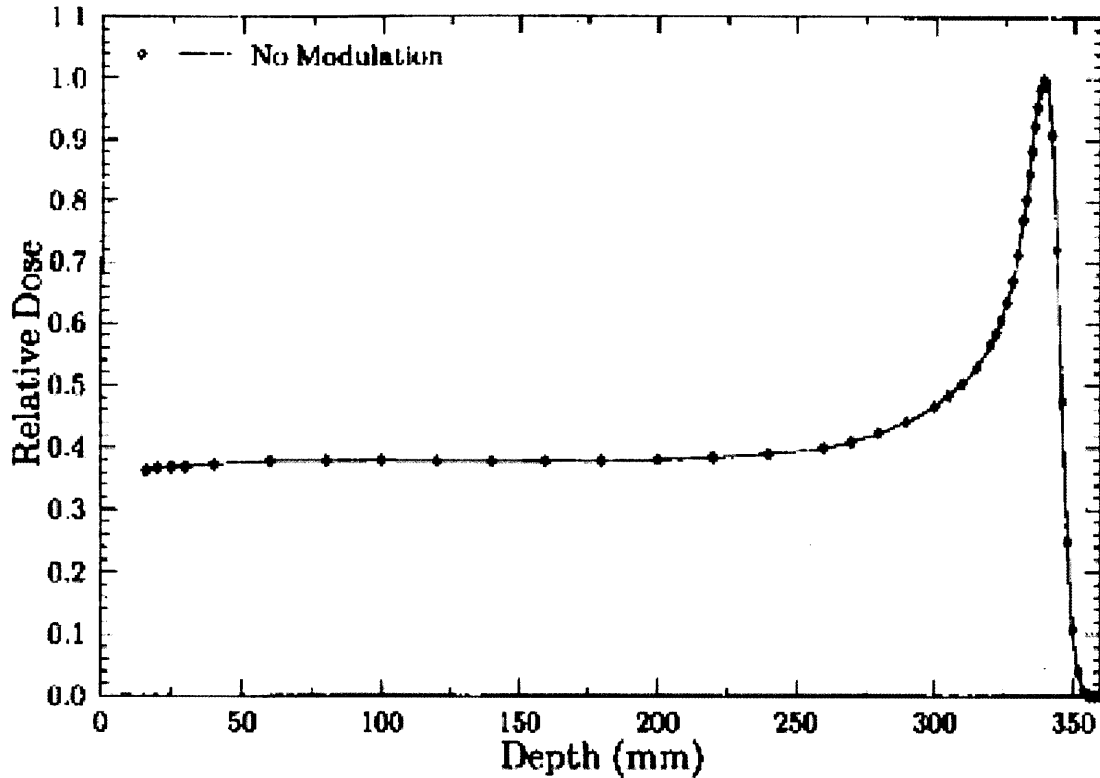
8

Figure 4. The Bragg peak. The dose deposited by a proton as a function of tissue depth; figure adapted from (4)

The Bragg peak (high dose area) can be quite narrow. However, the typical tumor dimension along the beam direction is usually not as narrow as the pristine Bragg peak, hence we need to spread out the Bragg peak. A spread out Bragg peak (SOBP) is generated by passing a monoenergetic proton through a range modulator, which spreads out the beam energy appropriately, to produce high dose region of a specific depth. Lower energy protons will stop at the shallowest point of the tumor, while the highest energy protons will stop at the deepest part of the tumor, as illustrated in Figure 5. The advantage of protons over photons is that protons stop distal to the tumor, while photons continue all the way to the other side of the body (see Figure 6 for comparison of photon and proton dose deposition). As with the case for multibeam photons, adding an additional proton

9

beam decreases the dose to the normal tissue as shown in Figure 7. Unlike photons, though, protons stop after the tumor and hence spare more normal tissue.
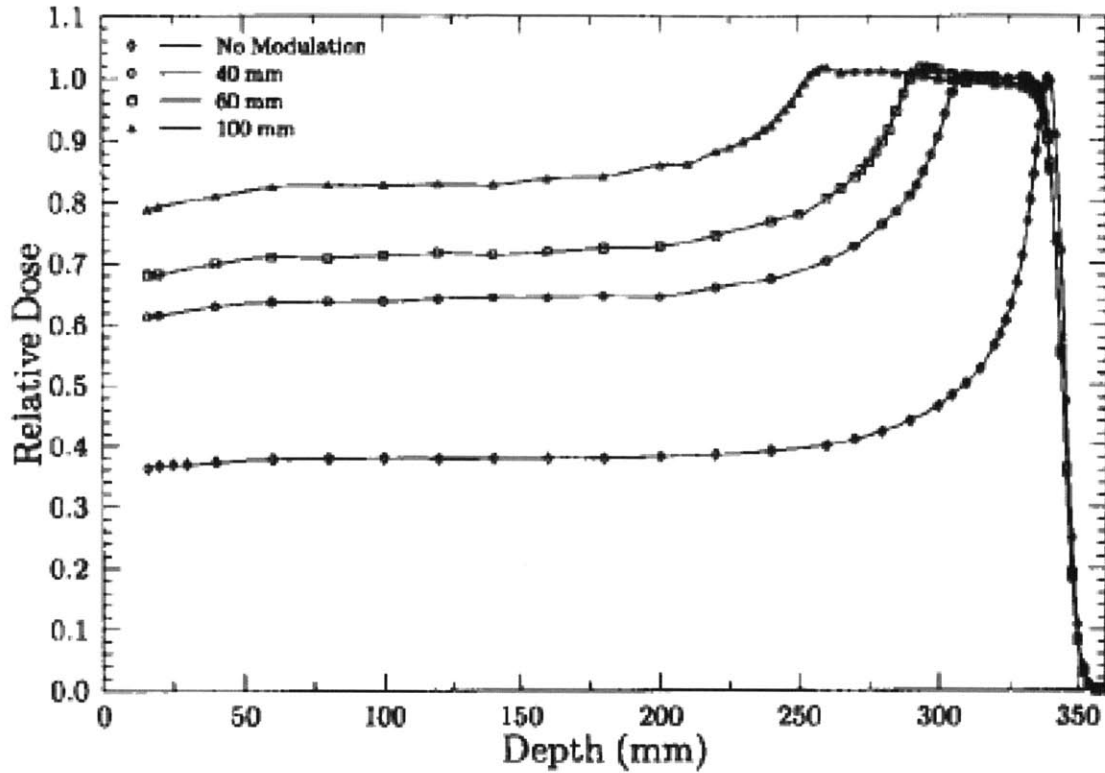

Figure 5. Spread out of the Bragg peak as a result of adding modulation to the original proton beam. As the beam is more modulated (more spread out in energy), protons travel to different depths and cover the entire tumor depth. Protons with lower energy stop closer to the skin and protons with higher energy travel deeper. The spread out in energy is represented as the spread out in wavelength of protons in the figure (figure adapted from 4)
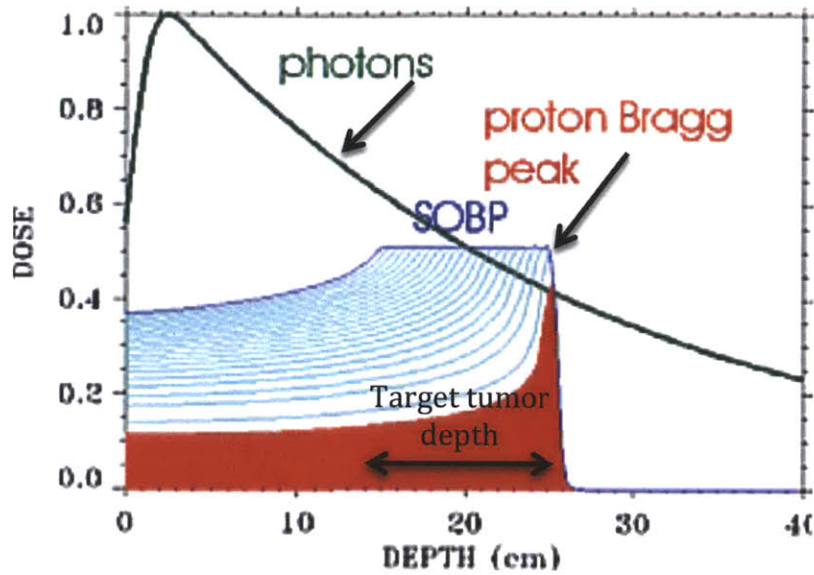
Figure 6. Comparison of spread out Bragg peak (SOBP) to photon dose deposition pattern. The Key difference is that protons stop distal to the tumor while photons continue to deposit energy. Additionally, protons have the advantage in the proximity to the skin over photons because protons deposit lower energy as they enter the body and their energy deposition increases towards the Bragg peak. Photons, on the other hand, deposit larger amount of energy to the region close to the skin than to the actual tumor. As a result photons deposit more energy to the normal tissue close to the skin than protons do; figure adapted from (7)
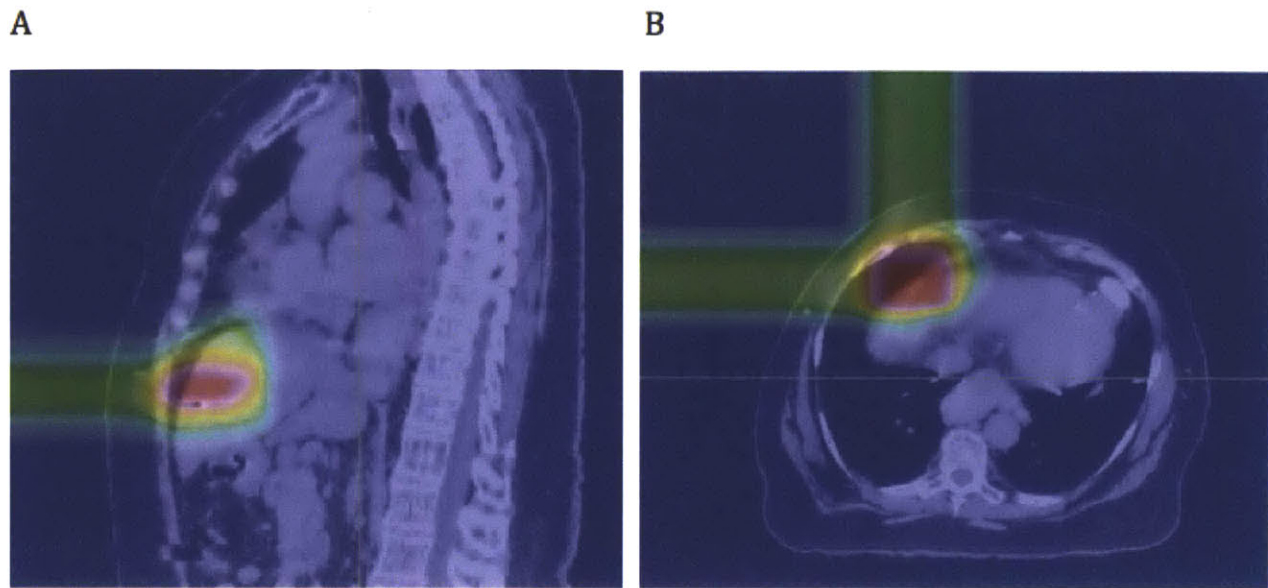
A   B

Figure 7. Proton dose deposition pattern as calculated based on the treatment plan in XIO, visualized in CERR. A: The proton beam stops after the tumor; B: Two orthogonal beams allow normal tissue to get only 50% of the tumor dose.

Metrics for quantifying dose to organs

Dose-volume histograms (DVHs) are extensively used in radiation treatment planning. The purpose of a DVH is to summarize the 3D dose distribution in a graphical 2D format. The "volume" referred to in DVH analysis can be the tumor target of radiation treatment, a healthy organ near a target, or an arbitrary structure.

DVH can be visualized in two different ways: differential that takes the appearance of a typical histogram, or cumulative. Bin doses are along the horizontal axis, and structure volumes (either percent or absolute volumes) are on the vertical (as shown in the top of Figure 8). The height of the column of the given bin indicates the volume or percentage volume of the structure receiving a dose given by that bin interval. A differential DVH is created by first determining the size of the dose bins of the histogram. Bins can be of arbitrary size, e.g. 0-1 Gy, 1.001-2 Gy, 2.001-3 Gy, etc. A

cumulative DVH is plotted with dose bins along the horizontal axis, as well. However, the column height of the first bin (0-1 Gy, e.g.) plots the volume of the structure receiving a dose equal to or greater than that dose. The column height of the second bin (1.001-2 Gy, e.g.) represents the volume of structure receiving greater than or equal to that dose, etc. With fine bin sizes, the cumulative DVH takes on the appearance of a smooth line graph (as shown in the bottom of Figure 8).
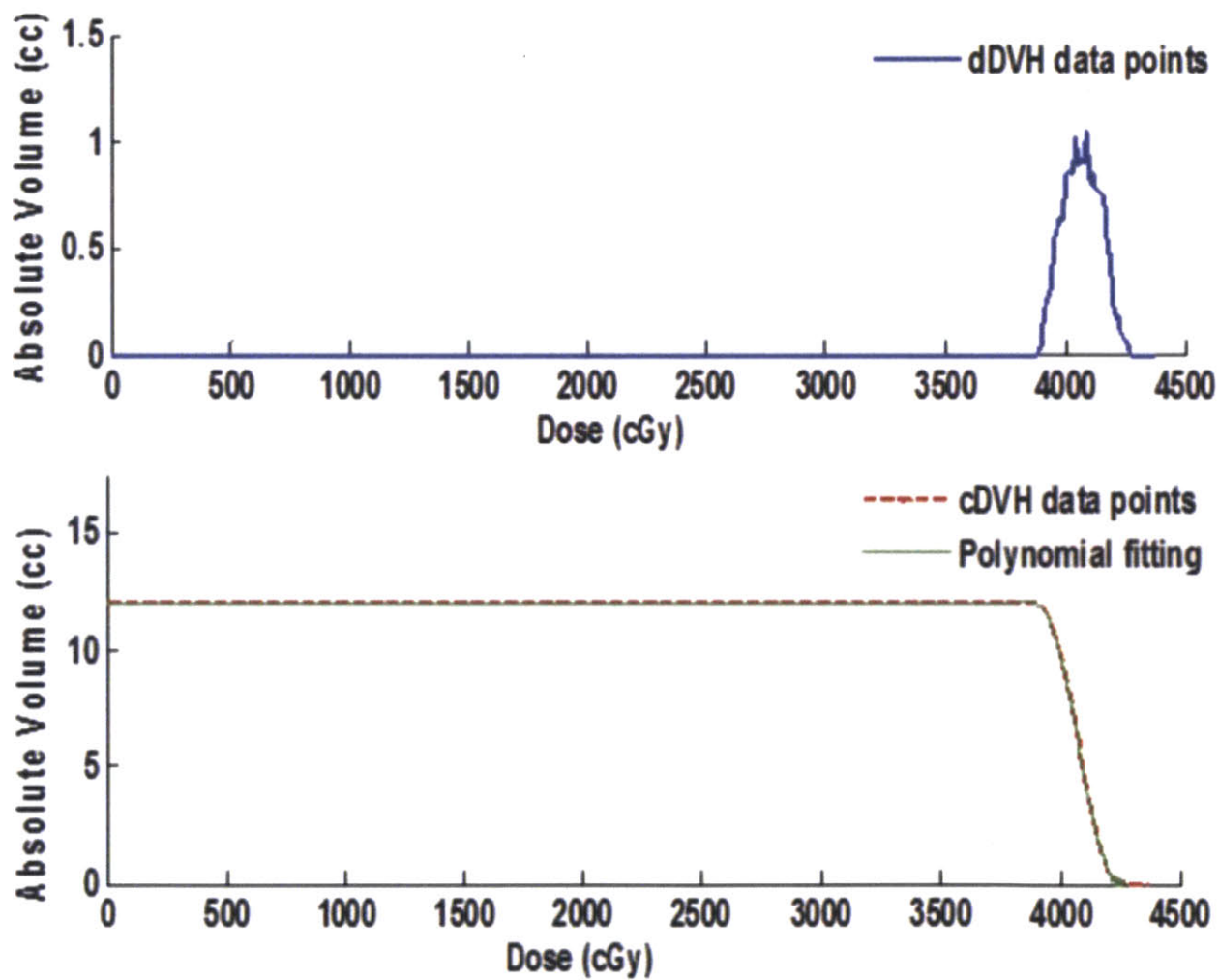

Figure 8. Dose Volume Histogram (DVH) principle. Top: differential DVH showing volume receiving a given dose; Bottom: cumulative DVH showing fraction of volume receiving a given dose or greater (figure adopted from 8).

Lyman's normal tissue complication probability (NTCP) (27) is a common means of comparing the relative goodness of rival treatment plans. The plan that produces the same tumor control probability (same dose to tumor) while sparing normal tissues (plan with lower NTCP) identifies the better plan. In Lyman's model, the NTCP increases sigmoidally with dose as shown in Figure 9. Increase of dose in the low dose range generally results in negligible change in NTCP. After some point, increases in the dose applied result in large changes in NTCP and quickly become lethal. Tumor control probability (TCP) describes a competing effect to NTCP. TCP is the probability that no malignant cells are left in a specified location after irradiation. This probability is used to determine an optimal treatment strategy where the dose to the tumor is increased without increasing the damaging effects of radiation of healthy tissues (9). Similarly to NTCP, TCP also assumes the sigmoidal shape. The optimal treatment planning would aim for the highest possible TCP while minimizing NTCP. The greater the separation of the TCP and NTCP curves, the higher local control can be achieved with lesser normal tissue complications. A shortcoming of NTCP is that it does not directly take into account the kind of tissue being irradiated, which clinically is very important — for example, if radiation to healthy tissue causes dry mouth with 20% probability then it is acceptable but if it causes myelitis and demyelination with 20% probability then such a radiation dose is not acceptable.
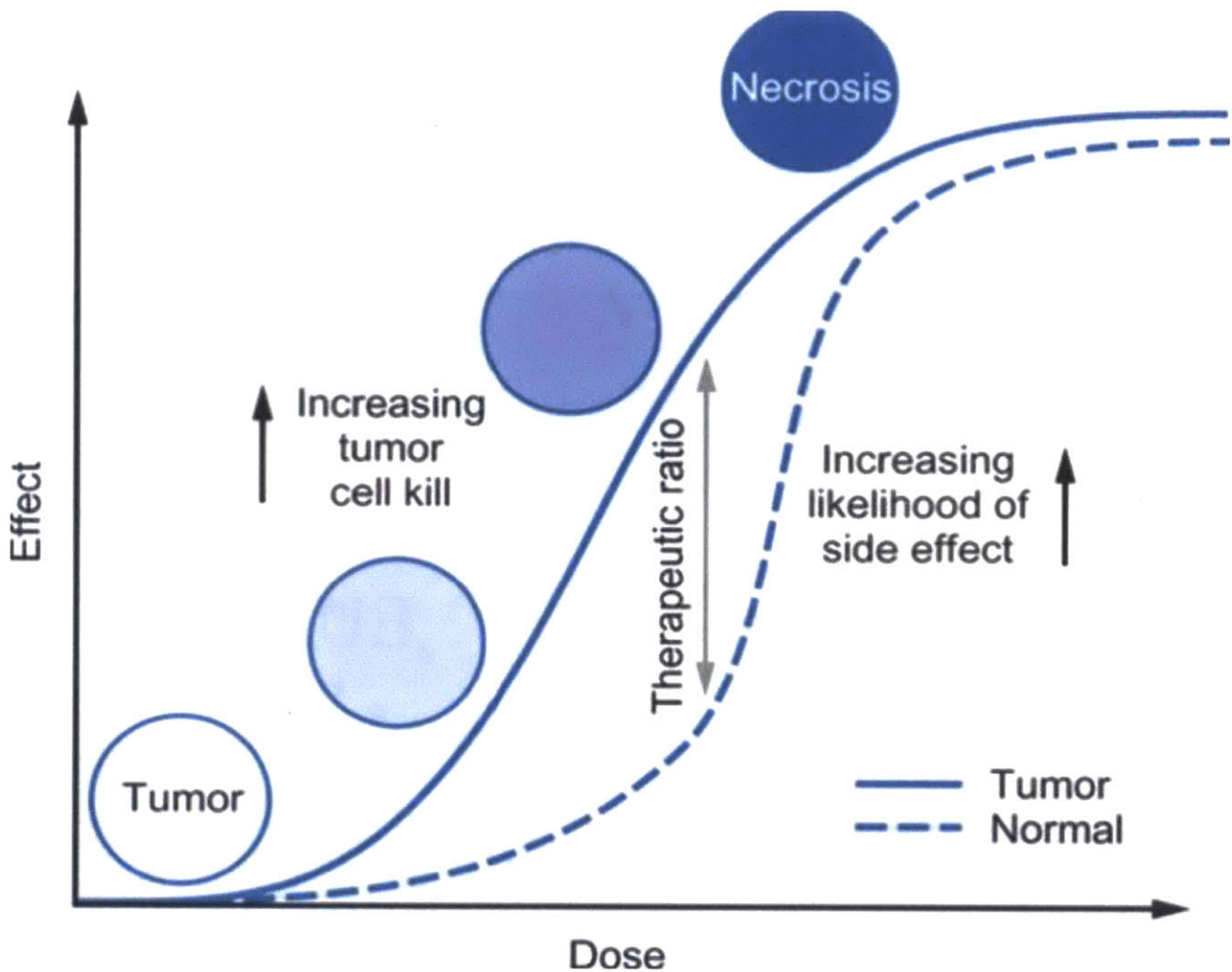
Figure 9. A schematic of NTCP as a function of dose. The effects on the y-axis correspond to the likelihood of complication (NTCP) (dashed line) and the probability of tumor control (solid line). As the dose increases, the effect increases. The optimal treatment is determined by maximizing TCP and simultaneously minimizing NTCP; figure adapted from (11)

Another metric to compare rival dose distributions is the *effective uniform dose* (EUD), which treats two dose distributions that deliver the same amount of radiation to a given area as equivalent regardless of the how the radiation is distributed within each area (12). Left part of Figure 10 shows a heterogeneous dose distribution (where some parts of the organ are irradiated more (D2) than other parts (D1)). This dose distribution results in a biological effect. The same biological effect can be achieved by irradiation of the whole organ to a uniform dose EUD, which is between D1 and D2.

The principle behind EUD is hence explained: the uneven dose distribution on the left is represented by the equivalent dose uniformly distributed over the same area as shown on the right. Unlike NTCP, which models the actual clinical complication probability and is calibrated by case studies, EUD is always well defined, and therefore makes a good comparison metric.
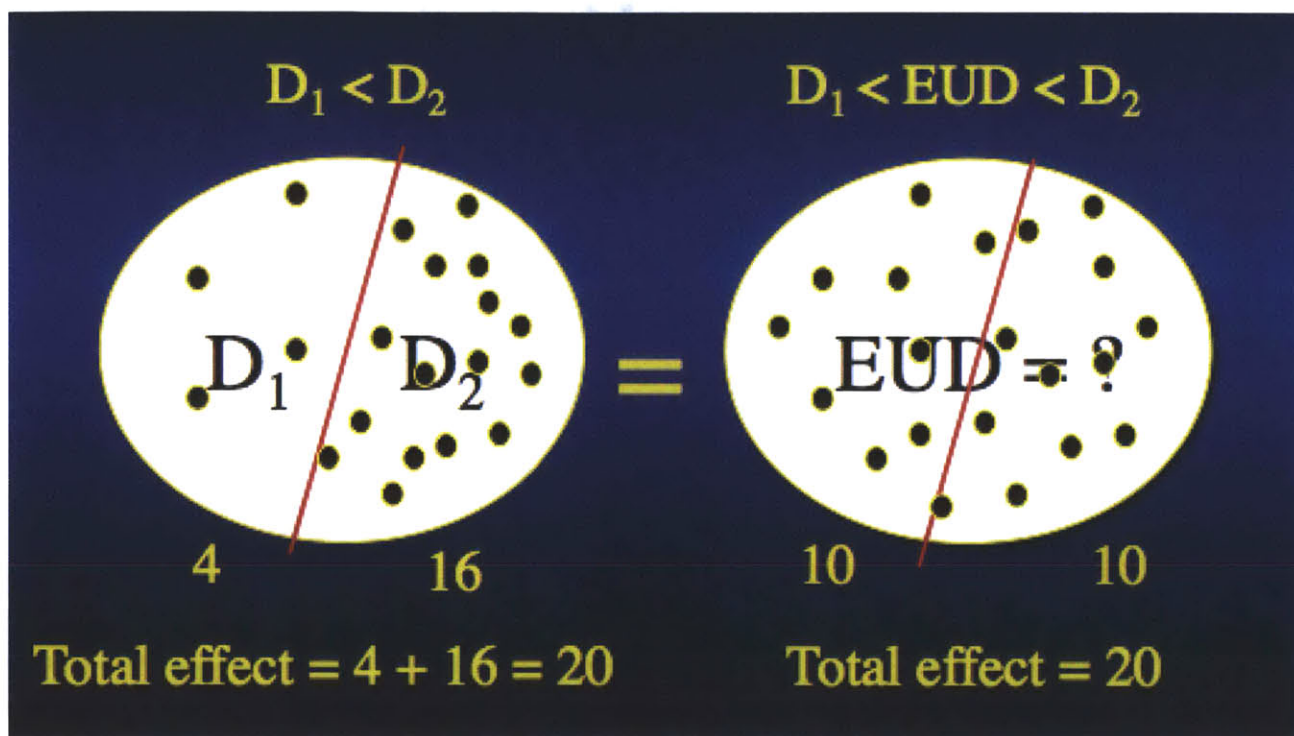

Figure 10. The concept of EUD as the equivalent dose. On the left the target is irradiated non-uniformly at two doses: D_1 and D_2. The same biological endpoint can be achieved by uniformly irradiating the dose to the equivalent uniform dose (EUD), which is between D_1 and D_2 (figure courtesy of A. Niemierko).

In this study, a current treatment planning method (3D) is compared to a newer approach (4D). 3D treatment planning calculates the dose distribution on static anatomy while it is being irradiated. That is not true as the tumor in many organs, e.g. in liver, moves with the organ itself due to respiration. The current solution to this problem is to enlarge the target volume (aperture) to accommodate motion of the tumor, as shown in Figure 11. This approach, however, is very misleading as it treats all shaded area, which in reality is normal tissue, as the tumor area. Hence the

16

plan does not calculate the dose delivered to the shaded region in the EUD for normal tissue because the region is treated as the target and not the tissue that should be saved.
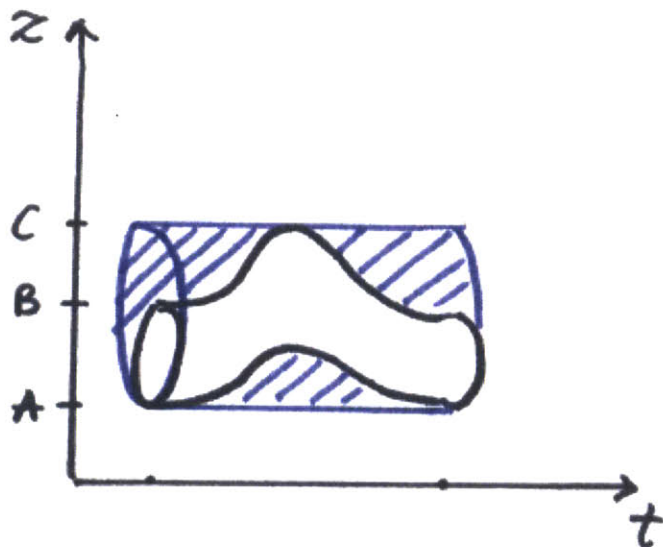

Figure 11. Superior-interior tumor motion as a function of time. The current 3D treatment planning enlarges the aperture to account for tumor motion, but during treatment planning the entire volume is treated as tumor, i.e., the shaded area is treated as dose to the tumor instead of dose to normal tissue. 4D treatment planning, on the other hand, is able to assign the dose delivered to the shaded area to normal tissue hence accounting for more damage to normal tissue than 3D treatment planning does.

In contrast to 3D treatment planning, the 4D approach explicitly takes into account that the shaded area is really normal tissue. Hence the volume taken to calculate EUD for normal tissue in 4D treatment planning includes the shaded region of high dose. This region is not included in 3D treatment planning, and, as a result, EUD to normal tissue is higher in 4D than in 3D treatment planning.

METHODS AND MATERIALS

We collected 25 sets of anonymized 4DCT data. The cohort consisted of hepatic tumor patients who were treated with two to four proton beams with prescribed doses ranging from 40–75Gy. Tumor and normal tissue contours were drawn by one physician (TS Hong), generally at the T30 breathing

phase. The treatment beam parameters used in 4D calculations were those used to actually treat the patient (same field directions, beam weights, field margins, etc.).

Subsequently, we loaded the 4DCT data from all 10 breathing phases (T00-T90) with the corresponding contours of the targets and the important structures (liver, kidney, stomach, etc.) together with the corresponding beam parameters, which include beam angles and weight, prescribed dose, distal margin, and the smearing radius, used in treatment into Aqualyzer (22) (the details of how Aqualyzer works are included in Appendix A), a research treatment planning system that uses the pencil-beam algorithm (23) to calculate the dose in 4D. Aqualyzer then calculates the compensating bolus based on all breathing phases. To generate 3D planning dose distributions, we replicated the data from phase T30 for all breathing phases and used the same dose calculation algorithm as for 4D. The volume-of-interest (VOI) contours were propagated to all the other breathing phases within Aqualyzer using Plastimatch deformable registration (24). Aqualyzer then calculated and returned the 4D dose distribution and the dose volume histograms (DVHs) for each patient for each of the structures (organs) for which the contours were provided.

The target for 4D treatment planning was defined by taking the target from the treatment plan performed by the commercial treatment planning program XIO (25) and applying the smear according to the prescription. Aqualyzer ensured that the target was fully covered in all breathing phases. For the 3D treatment planning calculation, the target was also defined as the target from the XIO plan, but it was whatever this target was at phase T30. Hence it did not account for the target movement. The smearing was applied as prescribed (an in depth description of Aqualyzer calculation details is attached in Appendix A).

Using the DVH for the accumulated dose (i.e., the dose summed over all the breathing phases) for both gated (T40–T60) and ungated scenarios, we computed the effective uniform dose (EUD) (12) as described in (27,26) based on a normalized dose of 60Gy (regardless of the actual dose prescribed) delivered in a 15-fraction schedule and corrected to 1.5Gy/fraction for all cases to avoid differences in EUD due to dose differences (with the parameters as follows: $\eta=2$, $RBE_{max}=1$, Lyman $n=0.97$). A sample spreadsheet of this calculation is attached in Appendix B.

To determine if the mean difference in EUD between 3D and 4D treatment planning, and between gated and ungated treatment, statistically differs from zero we performed one-sample t-tests. We used Pearson's correlation coefficient to evaluate the correlation between the mean difference in EUD and tumor size, as well as superior-inferior (S-I) motion.

RESULTS

Benchmarking 4D Treatment Planning

In order to validate Aqualyzer as a tool to plan treatment, we compared the 3D Aqualyzer treatment plans to those generated by XIO (28), a commercially established treatment planning program (see Table 1 for comparison between XIO and Aqualyzer). To compare the computed doses for each treatment plan, we used CERR (29) to create a dose subtraction image from the distributions computed by Aqualyzer and XIO, and visually evaluated the differences. A representative case is shown in Figure 12. Since the dose distributions are similar in all 3 views (coronal, sagittal and transverse), we concluded that Aqualyzer was sufficiently accurate and reliable and proceeded with the study.

Table 1. Comparison of XIO vs. Aqualyzer.

| Variable	XIO	Aqualyzer
Compensator design	Designed at T30; smeared	Designed based on all 10 phases
Distal Range Margin	5mm	5mm
Smearing	Depending on the patient 5mm-10mm	Depending on the patient 5mm-10mm
Temporal Resolution	Single phase-3D plan	10 phases-4D plan
Dose Algorithm	MGH pencil beam	NIRS/ MGH pencil beam
Target Contours	1 set drawn by MD on T30	Contours drawn by MD on T30 propagated to all phases using deformable registration
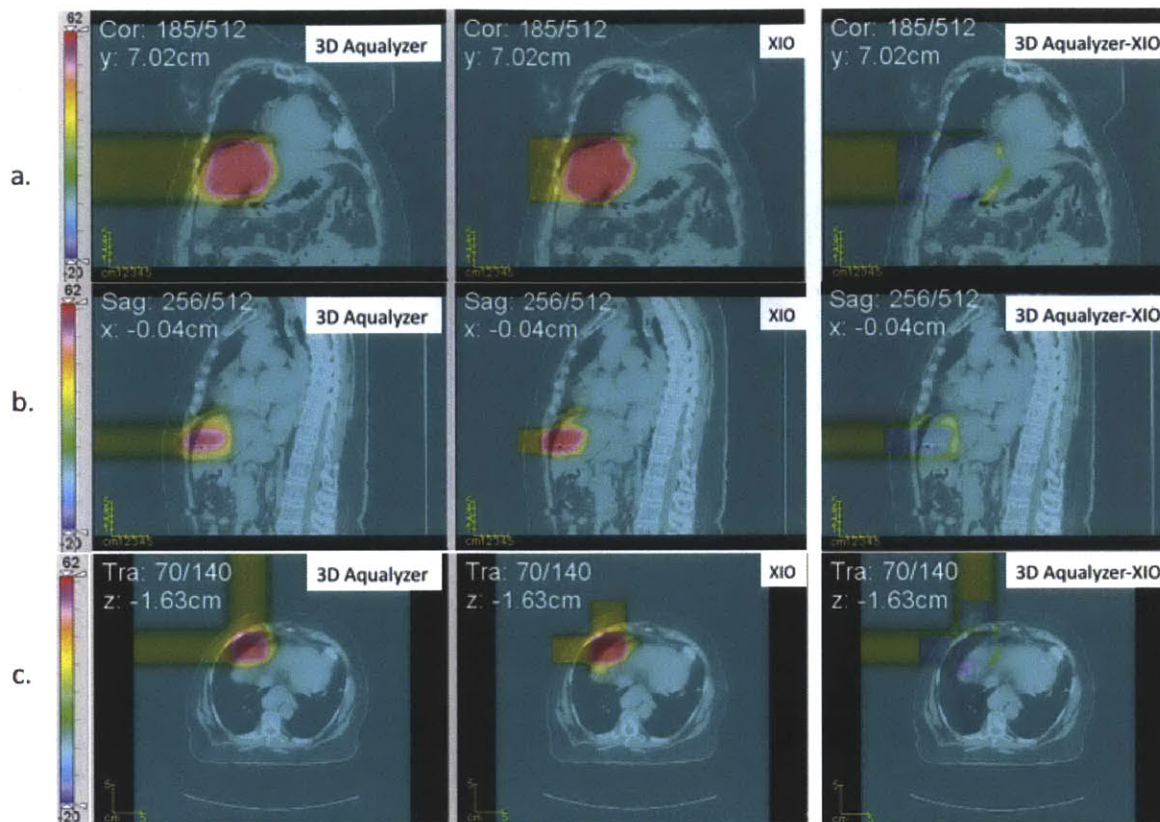
Figure 12. 3D Aqualyzer and 3D XIO plans' CERR subtraction images. (a) coronal view, (b) sagittal view, and (c) transverse view. The colorwash scale on the left is in units of Gy. The differences (in the rightmost column) are very small, which indicates that Aqualyzer dose distribution is similar to XIO plan. The yellow high dose areas outside of the body (in the rightmost column) result from XIO plan ending closer to patient's body than Aqualyzer plan.

4DCT Quality

In selecting cases for analysis we took into account the quality of the 4DCT scans. For each patient, we examined all 10 breathing phases and visually verified that the anatomy was artifact free. Two cases with significant 4DCT scan artifacts were excluded from the analysis. Figure **13** shows an example of a case rejected due to a poor CT scan, where exhale phase T50 (right) looks normal but inhale phase T00 shows severe liver shape artifacts at the diaphragm due to irregular respiration. Because 4D CT artifacts can significantly distort tumor position and introduce error into dose computations, such cases were excluded from the analysis.

21

a.
**Deformed Liver 13
Phase T00**
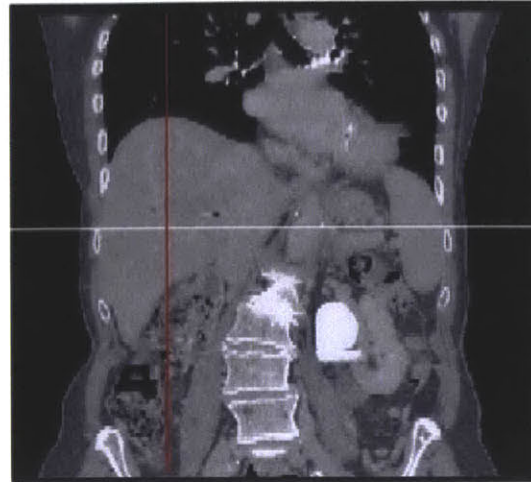
b.
**Normal looking Liver 13
Phase T50**

Figure 13. An example of a case rejected from the analysis. The CT scans shows anatomy at two different respiratory phases: (a) the liver at inhale (T00) is significantly deformed at the dome of the liver, while (b) at exhale (T50) the liver appears normal

EUD of Normal Liver

The EUD of normal liver for 4D and 3D treatment planning is shown in Figure 14 and Figure 15. Computing normal tissue irradiation based on 4DCT data always yielded a larger EUD than the equivalent computation based on 3D planning using a CT scan at breathing phase T30, with the mean difference of 3.8Gy (σ=1.9Gy, p<0.0001), or 15.1% of EUD for 4D ungated plan (σ=7.9%, p<0.0001). The difference in EUD between 4D and 3D planning for a representative case is shown graphically in Figure 16; the largest difference in the dose is in the inferior portion of the liver. 4D ungated planning always resulted in greater normal liver EUD than 4D gated planning (Figure 17 and Figure 18. A) with the mean difference of 2.9Gy (σ=1.9Gy, p<0.0001), 11.2% of EUD for 4D ungated plan (σ=5.1%, p<0.0001). The relative difference in the plans is also evident in the DVHs for 4D vs 3D plan and gated vs ungated plan (Figure 19).
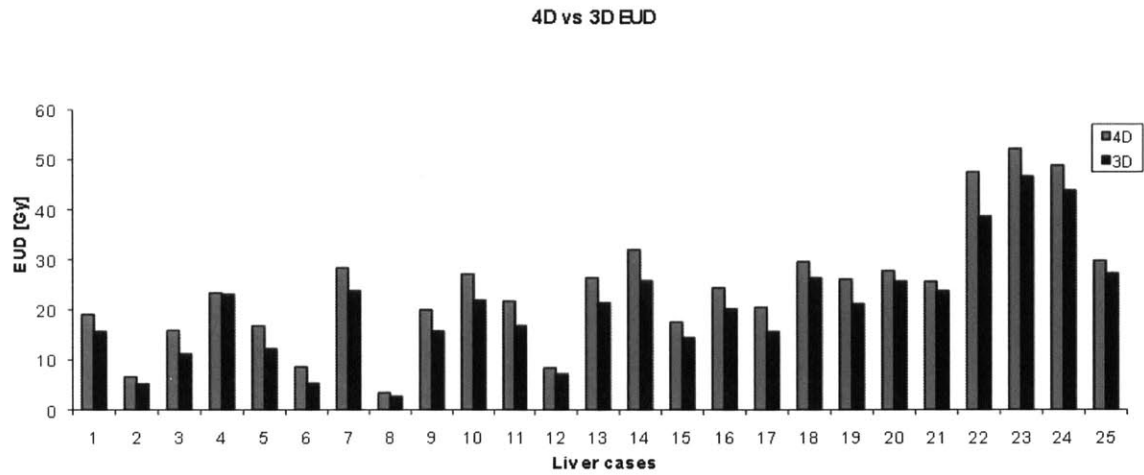
Figure 14. Comparison of 4D vs 3D treatment plan; the plot shows EUD [Gy] for 4D plan (gray) and 3D plan (black) for 25 patients. 4D treatment planning results in a higher EUD to normal liver.

4D vs 3D ΔEUD
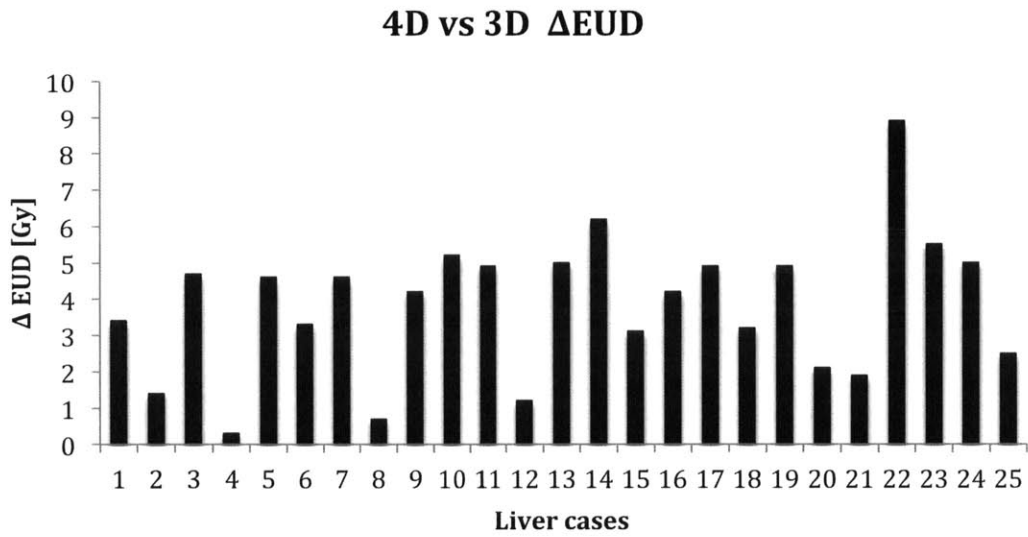
Figure 15. Difference between 4D and 3D treatment plan; the plot shows ΔEUD [Gy]= 4D EUD-3D EUD.

23
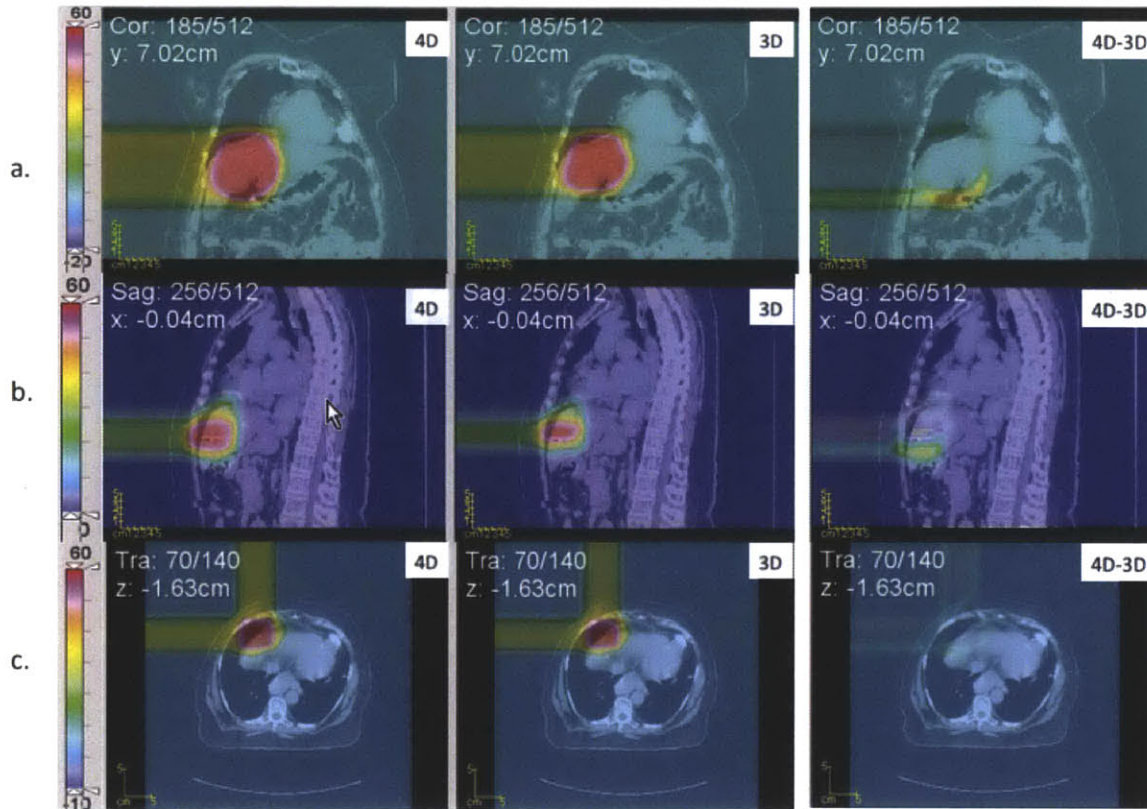
Figure 16. 4D ungated and 3D Aqualyzer plans' CERR subtraction images. (a) coronal view, (b) sagittal view, and (c) transverse view. The colorwash scale is in units of Gy.
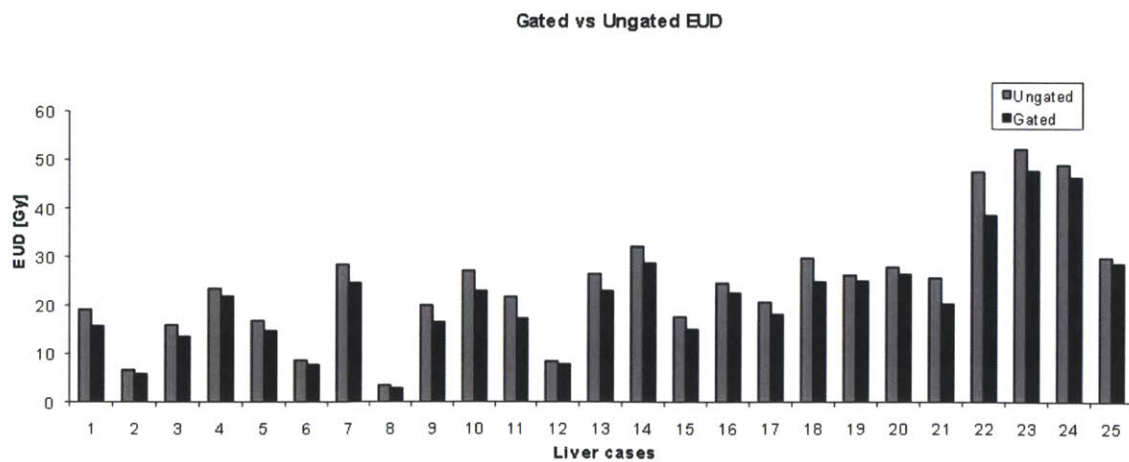
Figure 17. Comparison of 4D ungated vs 4D gated normal liver EUDs; the plot shows EUD [Gy] for 4D ungated plan (gray) and 4D gated plan (black) for 25 patients.

24
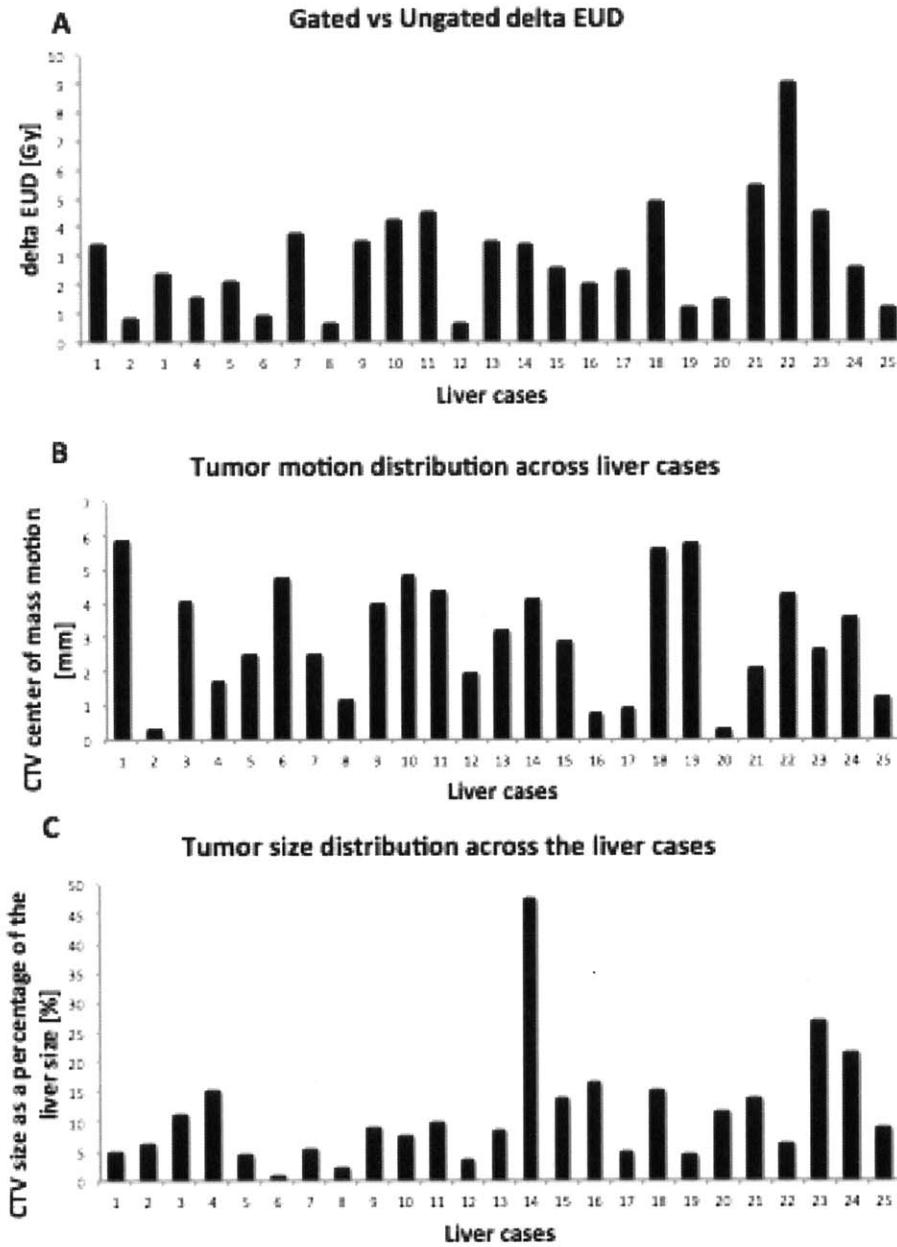
Figure 18. A. Difference between 4D and 3D treatment plan; the plot shows delta EUD [Gy]= 4D EUD-3D EUD; B. Tumor motion (S-I CTV center of mass motion) distribution across liver cases; C. Tumor size (CTV as a percentage of the respective liver volume) distribution across liver cases.

Gated Vs Ungated Vs 3D DVH for Liver-CTV
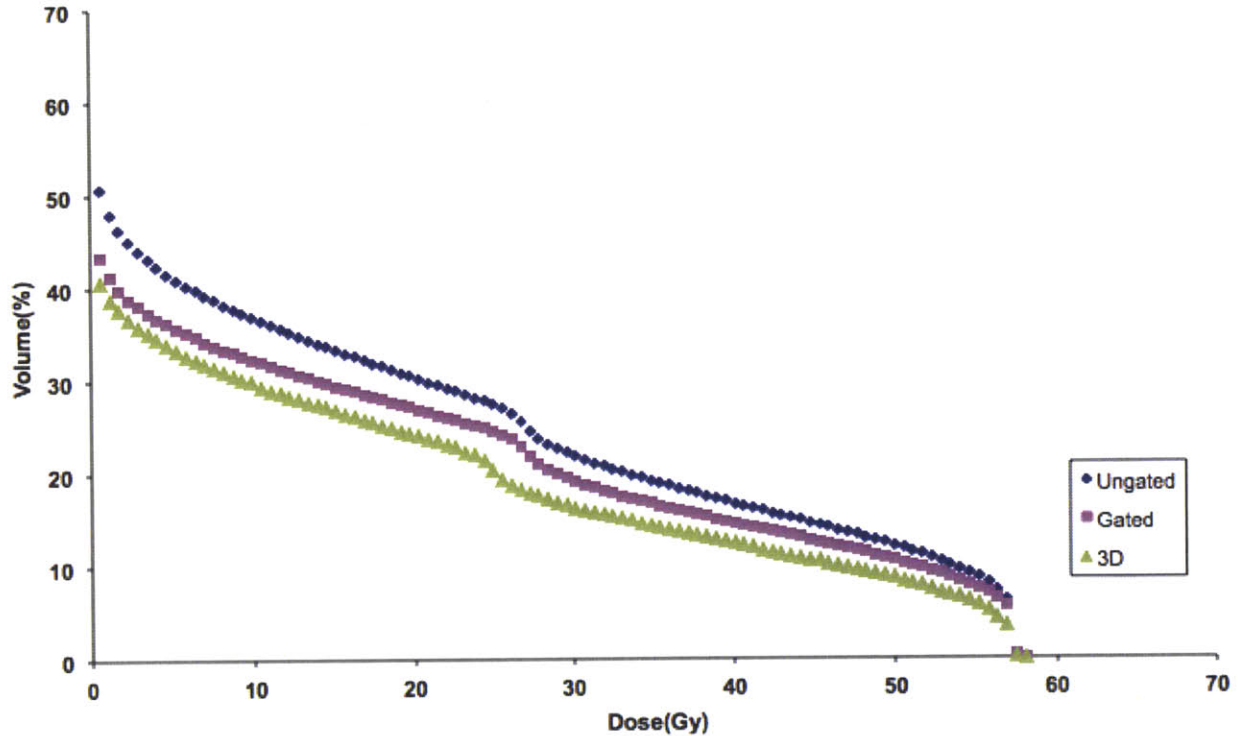
Figure 19. Comparison of cumulative DVH for 4D gated, ungated and for 3D plans for a representative liver case. The liver irradiated volume is the greatest for 4D ungated plan and the smallest for 3D plan.

Correlation between ΔEUD and Tumor Motion, Size and Position

A logical question to ask is if there is a correlation between the size of the change in EUD to normal liver and variables such as tumor motion amplitude, tumor size, or tumor location within the liver. These variables are plotted in Figure **18**. B,C. Since no obvious conclusion could be reached by just inspecting the data, we computed correlations between ΔEUD and CTV mean center of mass motion and between ΔEUD and CTV size. A weak correlation was observed between ΔEUD and CTV motion (r=0.59 for 4D/3D, r=0.48 for ungated/gated) and a much weaker correlation was observed with CTV size (r=0.31 for 4D/3D, r=0.26 for ungated/gated), see

Table **2**. The scatter plots of how ΔEUD varies with CTV motion and size are shown in Figure **20**.

Moreover, there is no evidence that the position of the tumor in liver influences ΔEUD (Figure **21**).

	CTV motion[*]	CTV size[=]
ΔEUD 4D vs. 3D plan [Gy]	0.59	0.31
ΔEUD ungated vs. gated plan [Gy]	0.48	0.26

Table 2. Correlation coefficients of ΔEUD with CTV motion[*] and size[†]

[*]CTV center of mass motion [mm]
[=] % of liver size
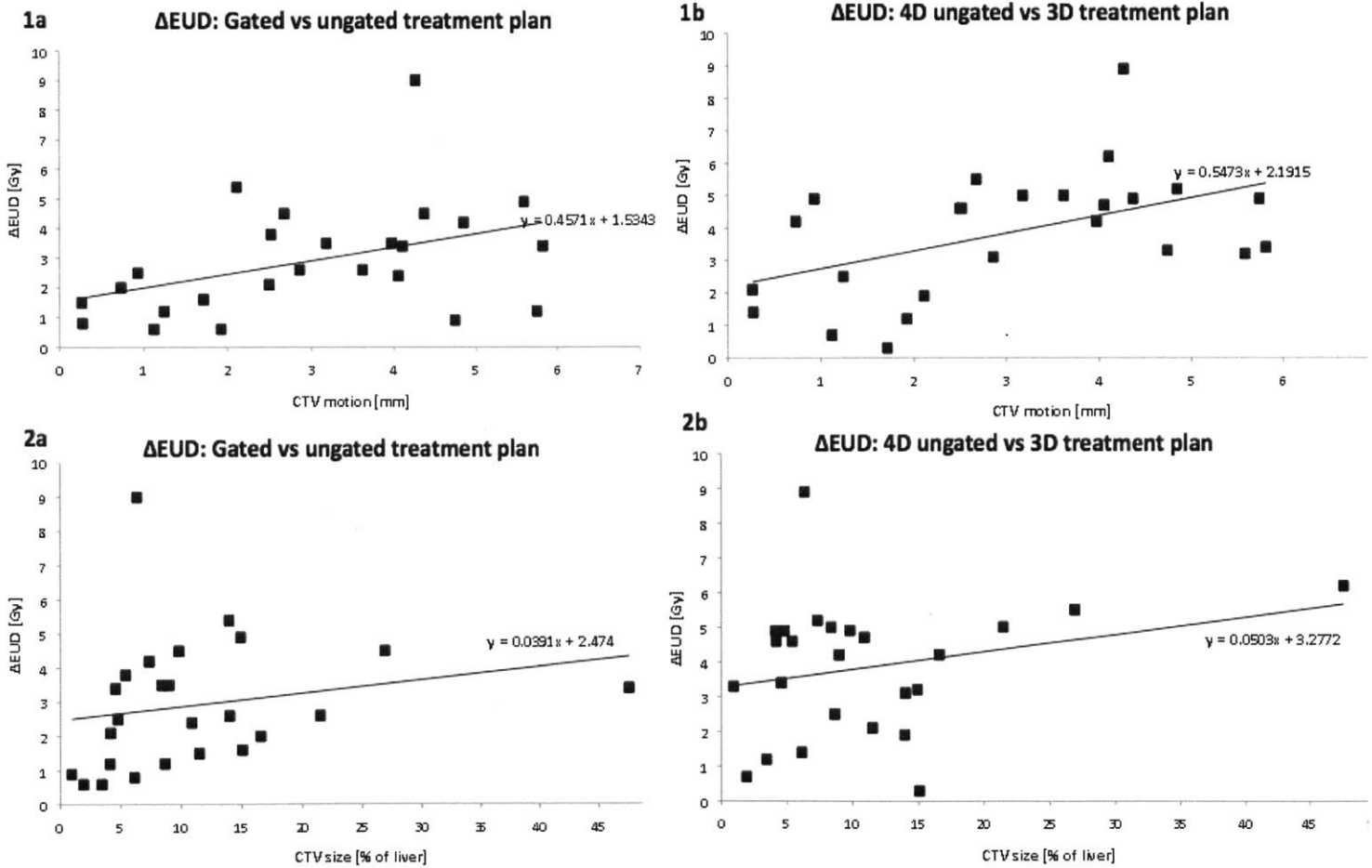
Figure 20. Scatter plots of ΔEUD as a function of CTV motion (1) and CTV size (2) for (a) gated vs ungated treatment and for (b) 4D vs 3D treatment.

ΔEUD based on tumor location
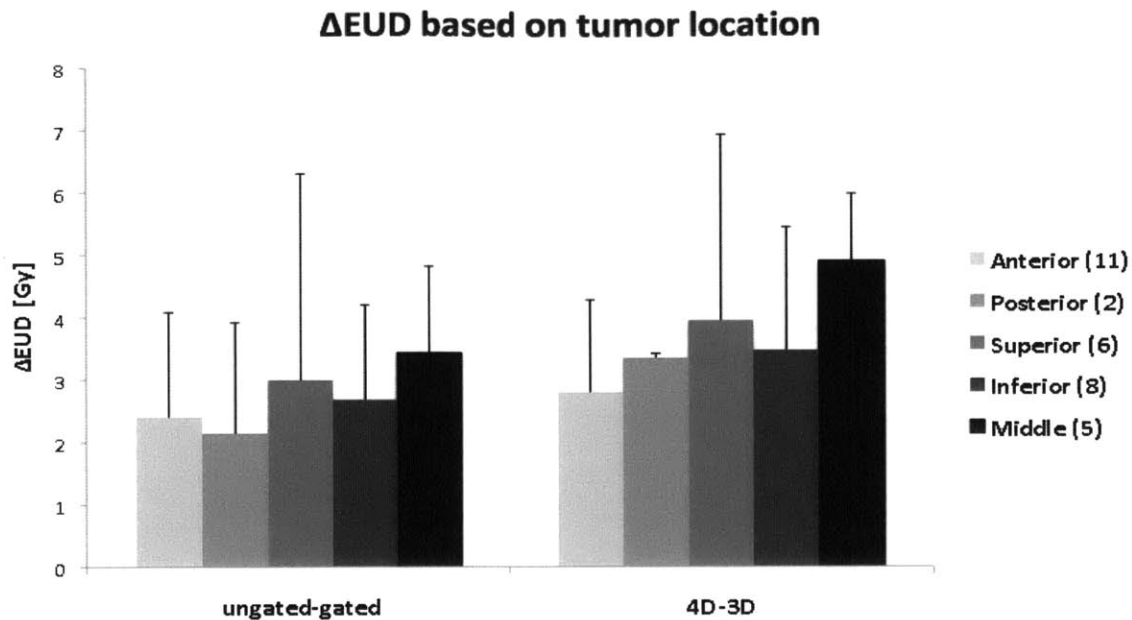
Figure 21. Dependence of ΔEUD on tumor location; the numbers in brackets following tumor location denote the number of cases of tumor at a given location; posterior tumors were included for completeness, but with only 2 cases no conclusions can be drawn.

Finally, NTCP was calculated for all cases and, although it was not used as a metric of comparison between 4D and 3D treatment planning, it revealed that our data follow the beginning of the Lyman model for low dose levels (see Figure **22**).

Normal liver NTCP as a function of dose
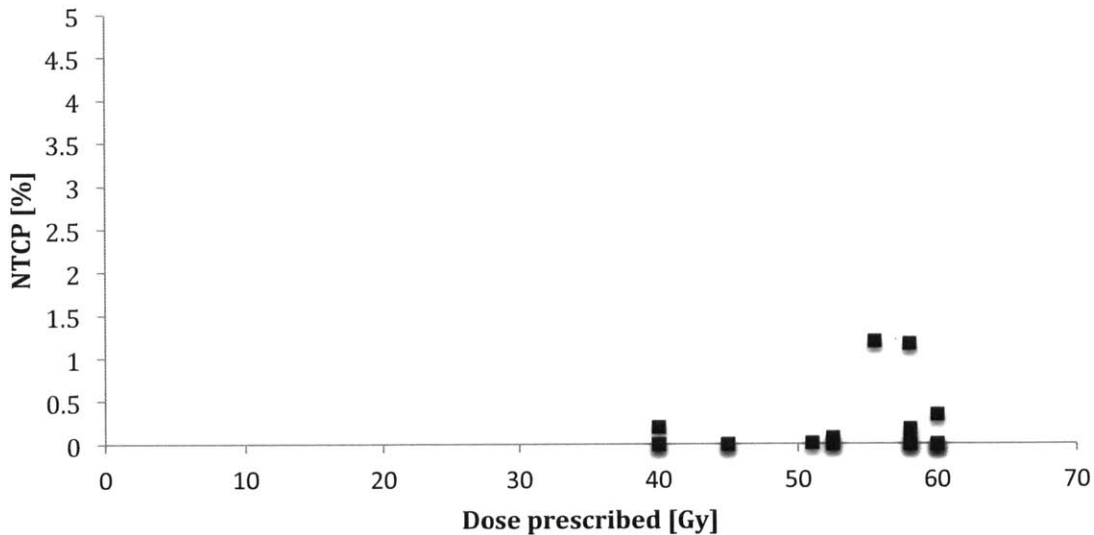
Figure 22. NTCP as a function of the prescribed dose calculated before dose normalization to 60Gy.

DISCUSSION

Accurate assessment of radiation doses delivered to target as well as normal tissue is critical in safe and effective radiation treatment. As shown in Figure 14, Figure 15, and Figure 16, dose distributions and EUDs calculated by static 3DCT-based treatment planning significantly differ from those computed by a 4D treatment planning. This finding is consistent with previous publications (20) and motivates the use of 4DCT-based treatment planning to improve the ability to predict the doses delivered to healthy liver tissue during the treatment.

Unlike Rosu et al (20), however, we found that static 3DCT-based planning always underestimates the dose to normal liver independent of tumor position (Rosu et al reported that, compared to their convolution-based mathematical model, for tumors in the superior liver static 3D planning overestimates the normal liver dose while for tumors in the inferior liver, static planning

29

underestimates the dose). Their model, however, only incorporated 1D motion while we also took into account right-left and anterior-posterior motions. Furthermore, their patients were treated with photons and our patients were treated with protons. Our data suggest that, in general, lower doses

	CTV motion*	CTV size=

should be prescribed to deliver the desired amount of radiation to the target area. This finding is especially significant for dose escalation studies, where the dose tends to be close to the upper tolerable limit, as it suggests that the actual dose delivered to the liver—and the consequent likelihood of complications—might be significantly higher than predicted using 3DCT-based planning and possibly exceed safe levels.

Gating is a technique that pauses the irradiation during the breathing phases that exhibit the most movement; in our simulation, radiation beams are applied only during phases T40–T60 of the breathing cycle. Although gating can potentially more accurately target the tumor and decrease the radiation dose delivered to healthy tissue, it also increases the treatment time, and results in fewer patients being treated per fixed time and the cost of treatment for each patient increases. Gating has been previously reported to have limited advantages for kidney, stomach, liver, and small bowel photon treatment (30). However, based on 4DCT data, we found that gating proton treatment reduced the dose to normal liver tissue by 2.9Gy (σ=1.9Gy) while keeping the dose delivered to the tumor the same (see Figure 17).

Not surprisingly, the inaccuracies of 3DCT-based planning as compared to 4DCT-based planning, as well as the effect of gating, increases as tumor motion increases (Figure 20,

30

ΔEUD 4D vs. 3D plan [Gy]	0.59	0.31
ΔEUD ungated vs. gated plan [Gy]	0.48	0.26

Table **2**). This makes sense because essentially the only difference between 4D and 3D planning is that 4DTP takes into account the movement and 3DTP does not: thus, if the tumor moves more, 4D planning accounts for more normal tissue that enters the beam's path during treatment. From a clinical perspective, this finding suggests that, given limited resources, hospitals wishing to balance patient volume and treatment quality might do so by prioritizing patients whose tumors move more during breathing for more expensive 4DCT-based planning or gated treatment while using more cost-effective 3DCT-based planning for patients whose tumors are relatively stationary.

As expected, the difference in EUD between 3DCT and 4DCT-based planning does not depend on tumor size; because the primary difference between 3D and 4D planning is in the accounting for tumor motion and not geometry, tumor size should not appreciably affect the EUD. On the other hand, although we expected tumor location to matter (because the superior and middle regions of the liver move more during breathing, and the inferior region moves least), the data available to us consisted of too few cases data to be conclusive: although this trend can be visually noticed in Figure **21**, no firm conclusions can be drawn because the standard deviations are too large.

EUD was chosen as the metric of comparison of 3D/4D and gated/ungated TP instead of the more commonly used normal tissue complication probability (NTCP) (27) because for most of our patients the doses to the liver were sufficiently low such that NTCP was close to 0 (see Figure 9). It is impossible to compare NTCP differences if for both 3D and 4D NTCP was 0. NTCP is a threshold metric and will stay at zero until a critical dose for a given fraction of liver irradiated is reached (as

shown in Figure 9), our NTCP computed values are at the beginning of the rise to the threshold value. As a result, we chose EUD because it is derived from the DVH and hence provides a metric, at the same time making the analysis much more straightforward. Both EUD and NTCP can be used to optimize tumor treatment (31), hence choosing EUD does not decrease the clinical application of our findings.

CONCLUSIONS

Because 3DCT-based radiation treatment planning does not account for tumor motion during breathing, it inaccurately estimates the radiation dose delivered to normal tissue. In this study, we have shown that 3D planning systematically underestimates the dose delivered to healthy liver tissue by an average of 3.8Gy (σ=1.9Gy) compared to doses estimated based on 4DCT data that treats each breathing phase independently.

Gating the radiation beams during some breathing phases results in lower radiation exposure of healthy tissue. Specifically, we found that applying treatment only during phases T40–T60 decreases the dose to delivered to normal liver tissue by an average of 2.9Gy (σ=1.9Gy).

Future work will include looking at the effect of 4D planning as compared to 3D planning in a different organ – the lung. The lung is interesting because of its very low density compared to other tissues. As a result, the small changes in the dose planning are predicted to influence EUD to normal organ (lung) much more than for liver. Besides, the lung moves, of course, during breathing which will enable us to look at the effect of tumor motion in full swing.

32

REFERENCES

1. Trikalinos T, Terasawa T, Ip S, *et al.* Technical Brief on particle beam radiotherapies for the treatment of cancer. *Slide Presentation from the AHRQ 2010 Annual Conference* September 2010
2. Bortfeld T. IMRT: a review and preview. *Phys. Med. Biol.* 2006;51:pp.R363-379
3. Gerber DE, Chan TA. Recent Advances in Radiation Therapy. *Am Fam Physician* 2008:78;pp. 1254-1262
4. Miller DW. A review of proton beam therapy. *Med. Phys.* 1995;22:pp.1943-1954
5. Hauer-Jensen M. Late radiation injury of the small intestine: Clinical, pathophysiologic and radiobiologic aspects-A review. *Acta Oncologica* 1990:29;pp. 401-415
6. TomoTherapy. http://www.tomotherapy.com/beamlet/beamlet007/ Retrieved on 5/19/2011
7. Advanced Cancer Therapy. http://www.advanced-cancer-therapy.org/science_proton.html Retrieved on 5/19/2011
8. Pyakuryal A, Myint WK, Gopalakrishnan M, *et al.* A computational tool for the efficient analysis of dose-volume histograms for radiation therapy treatment plans. *J Applied Clinical Medical Phys* 2010;11
9. Yorke E. Modeling the effects of inhomogeneous dose distributions in normal tissues. *Seminars in Radiation Oncology* 2001;11:197-209
10. Dawson A, Hillen T. Derivation of the tumor control probability (TCP) from a cell cycle model. *Journal of Theoretical Medicine* 2006;00: 1-27
11. Gynecologic Oncology. http://www.mdconsult.com/books/page.do?eid=4-u1.0-B978-0-323-02951-3..50029-7&isbn=978-0-323-02951-3&type=bookPage&from=content&uniqId=248071062-26 Retrieved on 5/19/2011
12. Niemierko A. Reporting and analyzing dose distributions: A concept of equivalent uniform dose. *Med Phys* 1997;24:103-110
13. Pan CC, Kavanagh BD, Dawson LA, *et al.* Radiation-associated liver injury. *Int J Radiat Oncol Biol Phys* 2010;76:S94-S100
14. McGinn CJ, Ten Haken RK, Ensminger WD, *et al.* The treatment of intrahepatic cancers with radiation doses based on a normal tissue complication probability model. *J Clin Oncol* 1998;16:2246-2252
15. Balter JM, Brock KK, Lam KL, *et al.* Evaluating the influence of setup uncertainties on treatment planning for focal liver tumors. *Int J Radiat Oncol Biol Phys* 2005;63:610-614
16. Wu QJ, Meyer J, Fuller J, *et al.* Digital tomosynthesis for respiratory gated liver treatment: clinical feasibility for daily image guidance. *Int J Radiat Oncol Biol Phys* 2011;79:289-296
17. Kubas A, Chapet O, Merle P, *et al.* Dosimetric impact of breath-hold in the treatment of hepatocellular carcinoma by conformal radiation therapy [Impact dosimétrique du blocage respiratoire dans le traitement du carcinome hépatocellulaire par irradiation de conformation]. *Cancer/Raadiotherapie* 2009;13:24-29
18. Wu QJ, Thongphiew D, Wang Z, *et al.* The impact of respiratory motion and treatment on stereotactic body radiation therapy for liver cancer. *Medical Physics* 2008;35:1440-1451

19. Coolens C, Evans PM, Seco J, *et al.* The susceptibility of IMRT dose distributions to intrafraction organ motion: an investigation into smoothing filters derived from four dimensional computed tomography data. 2006;33:2809-2818

20. Rosu M, Dawson LA, Balter JM, *et al.* Alterations in normal liver doses due to organ motion. *Int J Radiat Oncol Biol Phys* 2003;57:1472-1479

21. Wang X, Krishnan S, Zhang X, *et al.* Proton Radiotherapy for liver tumors: dosimetric advantages over photon plans. *Medical Dosimetry* 2008;33:259-267

22. Mori S, Chen GTY. Quantification and visualization of charged particle range variations. *Int J Radiat Oncol Biol Phys* 2008;72:268-277

23. Gustafsson A, Lind BK, Brahme A. A generalized pencil beam algorithm for optimization of radiation therapy. *Med Phys* 1994;21:343-356

24. Plastimatch. http://plastimatch.org. Retrieved on 4/12/2011

25. XIO Treatment Planning System. http://www.elekta.com/healthcare_international_xio.php. Retrieved on 5/18/2011

26. Deasy JO, Niemierko A, Herbert D, *et al.* Methodological issues in radiation dose – volume outcome analyses: Summary of a joint AAPM/NIH workshop. *Med Phys* 2002;29:2109-2127

27. Dawson LA, Normolle D, Balter JM *et al.* Analysis of radiation-induced liver disease using the Lyman NTCP model. *Int J Radiat Oncol Biol Phys* 2002;53:810-821

28. Xio treatment planning. http://www.elekta.com/healthcare_international_xio.php

29. Deasy JO, Blanco AI, Clark VH. CERR: A computational environment for radiotherapy research. *Med Phys* 2003;30:979-985

30. van der Geld YG, van Triest B, Verbakel WFAR, *et al.* Evaluation of four-dimensional computed tomography-based Intensity Modulated and Respiratory-Gated Radiotherapy Techniques for Pancreatic Carcinoma. *Int J Radiat Oncol Biol Phys* 2008;72:1215-1220

31. Thomas E, Chapet O, Kessler ML, *et al.* Benefit of using biologic parameters (EUD and NTCP) in IMRT optimization for treatment of intrahepatic tumors. *Int J Radiat Oncol Biol Phys* 2005;62:571-578

32. Keall PJ, Joshi S, Sastry Vedam S, *et al.* Four-dimensional radiotherapy planning for DMLC-based respiratory motion tracking. *Med Phys* 2005;32:942-951

33. Urie M, Goitein M, Wagner M. Compensating for heterogeneities in proton radiation therapy. *Phys Med Biol* 1984;28:553-566

APPENDIX

Appendix A. Details of experimental treatment planning system – Aqualyzer.

Commercial proton treatment planning (e.g. CMS XIO used at MGH) does not have the capability of performing 4D dose calculations. Aqualyzer is a 4 dimensional treatment planning system for proton beam therapy, written by Dr. Shinichiro Mori of the National Institute of Radiological Sciences, Chiba, Japan. The software development was begun when he was a postdoctoral fellow at MGH in 2007. Aqualyzer is designed to calculate the dose for moving targets. The software is not FDA approved, and therefore is not used for routine clinical use, but is used to better understand the impact of motion on proton dose distributions.

Aqualyzer consists of two major components – Aqualyzer and Aquaview. The main functions of Aqualyzer are to a) read in 4D CT data b) read in contours drawn by the radiation oncologist on a single phase of 4D CT data c) specify treatment parameters d) propagate these contours to all other phases of respiration correlated CT data e) calculate a bolus for range compensation f) calculate dose at each respiratory phase g) map these distributions back to a single reference CT phase h) calculate the composite dose and DVHs in the reference phase. The results are stored in a Results folder for a given 4D calculation with specific input parameters. Aquaview's primary function is to data browse through the 4D dose distribution and aid in understanding 4D dose calculations.

Highlights of the specific steps in 4D treatment planning are provided to give an overview of what is involved in 4D treatment planning.

a) Reading in 4DCT: A folder containing the 10 phases of respiratory correlated CT is read into Aqualyzer. The subfolders contain the CT slices at a specific phase, and are labeled T00, T10…..T90. T50 corresponds to exhale and T00 to inhale. Parts of the CT couch are semi-automatically eliminated since they are not part of the treatment couch.

b) XIO contours of the target and organs at risk are read in. These contours are drawn by the physician and treatment planner. For liver cases, typical contours segmented at T30 include:

- GTV – the gross tumor volume – tumor visible on CT
- CTV – the clinical target volume – an enlargement of the GTV, by an adequate margin that includes microscopic extent (typically 5mm)
- PTV – the planning target volume that includes an additional margin beyond the CTV that accommodates inclusion of the target in the presence of setup errors and motion.
- Critical structures such as the spinal cord, stomach, duodenum, entire liver, left and right kidneys, porta hepatis, and any radio-opaque clips that are inserted near the edges of the tumor.
- Boolean structures can be generated in the contouring step. For example we define normal liver NLIV as the whole liver minus the CTV.

c) Specify treatment parameters
- Beam direction: the user specifies which beam directions are to be used. Typically, an anterior field and a right lateral field are used for proton beam treatment of liver tumors. In some cases, the fields are obliqued to avoid an anatomical feature (e.g. an oblique field may avoid the GI tract, which the anterior field would hit). Occasionally a 3 field plan is used. Choice of field direction is based on the experience of the dosimetrist and the physician's directive. The beam angles used in this analysis are the same as those used in the actual patient treatment.
- Other treatment parameters are discussed below

d) Deformable image registration: 4D CT data contains 10x more image data than a standard 3DCT. It is unrealistic to manually segment the target and normal anatomy for 4D treatment planning. Therefore, Aqualzyer uses the software *Plastimatch* (24), written by Dr. Gregory Sharp of MGH. Plastimatch calculates the vector transformation from one CT phase to another on a voxel by voxel basis. These transformations are then applied to the manual contours of organs drawn by the physician, to "map" the contour to all other phases of the respiratory correlated CT scan. This makes 4D treatment planning possible, since contours are needed at each phase for treatment planning. The end result of this step is that one has a volumetric contour of each structure (e.g. target, right kidney) at each respiratory phase.

e) Calculate a bolus and aperture for a 4D structure: the strategy for designing a compensating bolus is to define it such that the target is always adequately irradiated. Not doing so could lead to under-irradiation of the target during changes in radiologic pathlength during breathing. Therefore, a composite compensating bolus is designed from the 10 contours of the target. The bolus thickness chosen is the thinnest along a ray through all 10 phases of CT data to the distal target from a given beam direction. This guarantees that in the presence of motion, the proton beam reaches the distal edge of the target. The union of the 10 targets in the beam's eye view plane ensures that the aperture is sufficiently large to cover the target should it move in the aperture plane. Typically a 5mm range margin is used distally as a safety margin.

One additional parameter used in bolus design is important to point out. We include a "smearing" radius, typically 5-8mm. This smearing was originally suggested by Urie et al (33) as a way of ensuring target coverage in the event the compensating bolus and the target are misaligned during fractionated treatment. An exact nominal ray trace ensures distal range coverage with no uncertainty in bolus / target alignment. Smearing is achieved by choosing the thinnest radiological pathlength along neighboring rays within a 5mm/8mm radius. The smearing magnitude can be specified specifically along the x and y axes (z being along depth) should there the possibility of assymetric uncertainty.

Other treatment parameters:
One can specify the width of the gating window. Our typical assumption is that gating is performed in the T40-T60 window. This can be changed in the treatment parameter panel.

Prescription dose in Gy may be specified. The DVHs and isodose distributions are ususally displayed as percentages, 100% being normalized to the prescription dose.

Beam weight: relative dose contribution to isocenter is specified by this standard treatment planning parameter.
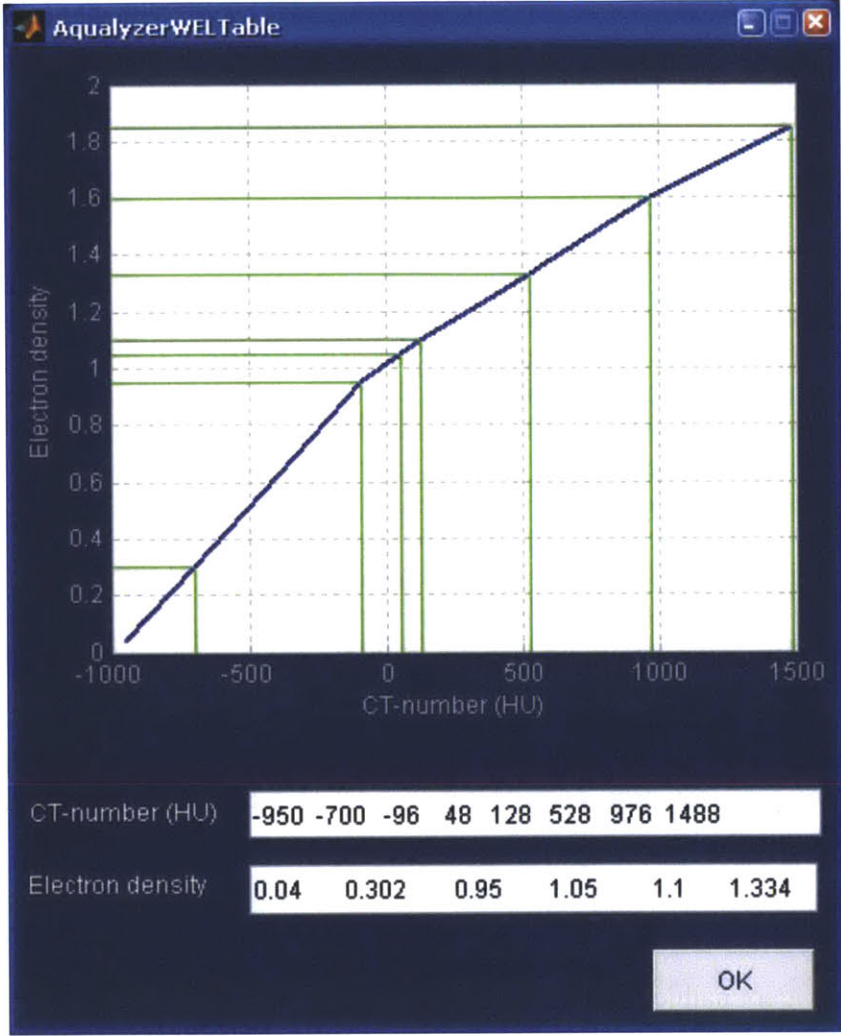
f) Dose calculation at each phase: with the compensating bolus specified by the analysis of target motion in 10 phases, dose calculations at each phase are then performed. The software is designed to operate in a multi-cpu environment. Most calculations are performed on a PC with a dual quad core processor. Dose calculations may require 1 hr. The end result is a set of 10 dose calculations, one for each respiratory phase. The dose distributions at this point are called the "room's eye view" dose distributions, reflecting what one would see when both anatomy and dose move in the room coordinate system.

g) Mapping dose back to the reference CT phase: We map the dose distribution from each respiratory phase back to a reference phase (typically the phase on which the physician drew the target). This step reduces the graphical data spread over multiple spatial instances to one spatial instance. The dose distribution in this space is called the "deformed dose". In this coordinate system, the anatomy is static, but the isodose distribution varies with time. This is sometimes also referred to as the organ's eye view; it is somewhat analogous to being in a glass elevator. You may feel you are not moving, but see the floors pass by as the elevator moves up/down.

h) Finally, we integrate the moving dose distribution over time, resulting in the "accumulated dose distribution". The endpoint is a static, composite dose distribution over static anatomy. We can now proceed with calculation of a DVH for an organ, as done in 3D treatment planning.

Miscellaneous:

Conversion from HU to water equivalent pathlength:

A CT scan provides a map of linear attenuation coefficients of the tissue relative to the linear attenuation coefficient of water at the nominal scan energy (effective x-ray energy). Both the electron density and effective atomic number of the material (and photon energy) determine the u. On the other hand, dE/dx of a charged particle is primarily dependent on the electron density (with a logarithmic dependence on the atomic number). To map the CT scan to a map of electron densities that is needed to calculate proton penetration, a simple calibration curve is used, as shown in Figure XX. In this figure, the y axis is the relative electron density, and the x-axis is the HU from the CT scan. Point of inflection is seen near 0HU, and approximates the dependence on Z for tissues found in the body.

Aquaview facilitates browsing through the several GB of data generated by Aqualyzer. These data include: a) composite and single field dose distributions in the room's eye view b) composite and single field dose distributions in the deformed (organ's eye) coordinate system and c) composite and single field distributions in the accumulated frame of reference. Aquaview also facilitates generation of movies to show dynamic dose distributions in the room and organ's eye view. It exports excel spreadheets of the dose volume histograms. These DVHs are then used to calculate the equivalent uniform dose (EUD) to tumor and normal tissues.

AqualyzerWELTable

| CT-number (HU) | -950 -700 -96 48 128 528 976 1488 |

| Electron density | 0.04 0.302 0.95 1.05 1.1 1.334 |

OK

Another feature of the Aqualyzer 4D plan is the capability to batch multiple patients in a run. After initial dose plan setup, multiple dose distributions for multiple patients can be run overnight or over the weekend.

Appendix B. Example of part of the spreadsheet used for EUD calculation.

		Num. of fractions = 15		Lyman n* = 0.97		Lyman m* = 0.12
		Dose_Ref (Gy) = 1.5		a = 1.03		TD_50* (Gy) = 39.8
		Alpha/Beta = 2				
		RBE_max = 1		* RILD 4 primarys (Michigan) 200 cGy/fx		
(1) cumulative DVH		**(2) NTD & diff. DVH**		**(3) EUD**		**(4) Lyman NTCP**
Dose (Gy)	cum. Vol. (%)	NTD_x (Co-Gy)*	fractional Vol.	$v_i D_i^a$	gEUD (Gy)	NTCP (%)
0	100	0.00	7.6E-01	0.0E+00	6.6	0.00
0.675	23.69541862	0.39	1.6E-02	6.1E-03		
1.35	22.10546006	0.81	1.1E-02	8.6E-03		
2.025	21.02678229	1.24	8.3E-03	1.0E-02		
2.7	20.19319315	1.68	7.5E-03	1.3E-02		
3.375	19.44018111	2.15	7.2E-03	1.6E-02		
4.05	18.72218172	2.63	6.1E-03	1.7E-02		
4.725	18.11017957	3.13	5.9E-03	1.9E-02		
5.4	17.52263832	3.64	5.5E-03	2.1E-02		
6.075	16.97730412	4.17	5.4E-03	2.3E-02		
6.75	16.43964393	4.73	5.0E-03	2.5E-02		
7.425	15.94419078	5.29	5.1E-03	2.9E-02		
8.1	15.43195073	5.88	4.8E-03	3.0E-02		
8.775	14.95136597	6.48	4.8E-03	3.3E-02		
9.45	14.46646458	7.10	4.9E-03	3.7E-02		
10.125	13.97292994	7.74	4.6E-03	3.8E-02		
10.8	13.51440795	8.39	4.5E-03	4.0E-02		
11.475	13.06835623	9.07	4.5E-03	4.4E-02		
12.15	12.6146305	9.75	4.0E-03	4.2E-02		
12.825	12.21078582	10.46	4.1E-03	4.6E-02		
13.5	11.79734863	11.19	3.9E-03	4.7E-02		
14.175	11.40597422	11.93	3.9E-03	4.9E-02		
14.85	11.02083493	12.69	3.7E-03	5.1E-02		
15.525	10.64768629	13.46	3.5E-03	5.2E-02		
16.2	10.29276341	14.26	3.4E-03	5.2E-02		
16.875	9.955586678	15.07	3.1E-03	5.0E-02		